

Robust SAC-Enabled UAV-RIS Assisted Secure MISO Systems With Untrusted EH Receivers

Hamid Reza Hashempour, Le-Nam Tran, *Senior Member, IEEE*, Duy H. N. Nguyen, *Senior Member, IEEE* and Hien Quoc Ngo, *Fellow, IEEE*

Abstract—This paper investigates secure downlink transmission in a UAV-assisted reconfigurable intelligent surface (RIS)-enabled multiuser multiple-input single-output network, where legitimate information-harvesting receivers coexist with untrusted energy-harvesting receivers (UEHRs) capable of eavesdropping. A UAV-mounted RIS provides blockage mitigation and passive beamforming, while the base station employs zero-forcing precoding for multiuser interference suppression. Due to limited feedback from UEHRs, their channel state information (CSI) is imperfect, leading to a worst-case secrecy energy efficiency (WCSEE) maximization problem. We jointly optimize the UAV horizontal position, RIS phase shifts, and transmit power allocation under both perfect and imperfect CSI, considering discrete RIS phases, UAV mobility, and energy-harvesting constraints. The resulting problem is highly nonconvex due to coupled channel geometry, robustness requirements, and discrete variables. To address this challenge, we propose a soft actor-critic (SAC)-based deep reinforcement learning framework that learns WCSEE-maximizing policies through interaction with the wireless environment. As a structured benchmark, a successive convex approximation (SCA) approach is developed for the perfect CSI case with continuous RIS phases. Simulation results show that the proposed SAC method achieves up to 28% and 16% secrecy energy efficiency gains over SCA and deep deterministic policy gradient baselines, respectively, while demonstrating superior robustness to CSI uncertainty and stable performance across varying transmit power levels and RIS sizes.

Index Terms—Physical-layer security, nonlinear energy harvesting, secrecy energy efficiency, successive convex approximation (SCA), soft actor-critic (SAC), deep reinforcement learning (DRL).

I. INTRODUCTION

THE increasing demand for secure, energy-efficient, and reliable wireless connectivity in beyond-5G networks has motivated the integration of unmanned aerial vehicles (UAVs) with reconfigurable intelligent surfaces (RISs) [1]. By combining aerial mobility with programmable electromagnetic wave manipulation, UAV-mounted RISs provide a flexible means to overcome blockage, reshape wireless propagation environments, and enhance downlink transmission quality. In particular, the ability to dynamically adjust both spatial

Hamid Reza Hashempour and Hien Quoc Ngo are with the Center for Wireless Innovation (CWI), Queen's University Belfast, BT3 9DT Belfast, U.K., (Email: {h.hashempour, hien.ngo}@qub.ac.uk).

Le-Nam Tran is with the School of Electrical and Electronic Engineering, University College Dublin, Belfield, Dublin 4, D04 V1W8, Ireland (Email: nam.tran@ucd.ie)

Duy H. N. Nguyen is with the department of Electrical and Computer Engineering, San Diego State University, San Diego, CA 92182, USA. (Email: duy.nguyen@sdsu.edu).

location and reflective behavior enables the formation of strong cascaded links that are difficult to achieve with static infrastructure. These advantages have triggered growing interest in the security aspects of UAV-RIS-assisted communication systems. For instance, machine-learning-based countermeasures against malicious attacks in UAV-assisted RIS networks are studied in [2], while robust secure transmission strategies under eavesdropping and jamming are investigated in [3] and [4].

Simultaneous wireless information and power transfer (SWIPT) further extends this paradigm by enabling radio-frequency (RF) signals to convey information and energy simultaneously. RIS-assisted SWIPT systems have been widely studied to enhance energy harvesting (EH) efficiency [5], [6]. However, when EH receivers are untrusted, they may opportunistically eavesdrop on confidential information, posing serious security risks [7], [8]. In practice, such untrusted energy-harvesting receivers (UEHRs) often provide imperfect or outdated channel state information (CSI), which renders secrecy-aware resource optimization particularly challenging.

Recently, deep reinforcement learning (DRL) has emerged as a powerful tool for solving highly nonconvex optimization problems in RIS- and UAV-assisted wireless networks. Existing studies have applied DRL to jointly optimize beamforming, power allocation, RIS configuration, and mobility for improving secrecy or energy efficiency in Internet of Vehicles (IoV) networks [9], movable antenna and STAR-RIS-assisted SWIPT systems [10], and active-RIS-enabled cognitive and energy-harvesting networks [11], [12]. These works demonstrate that DRL-based approaches can outperform conventional alternating optimization methods, particularly in dynamic and high-dimensional environments. DRL-based secrecy energy efficiency (SEE) optimization has also been investigated in RIS-assisted networks with trusted receivers and perfect CSI (PCSI) assumptions [13], where DRL is shown to effectively handle coupled power control and RIS configuration. In addition, DRL-based physical-layer security has been explored in emerging communication paradigms such as near-field MIMO systems [14], and RIS-assisted ISAC [15] and RIS-assisted energy-harvesting networks [12]. These studies highlight the potential of DRL for handling complex resource allocation problems.

Despite these advances, most existing works focus on secrecy rate or SEE under idealized assumptions, consider trusted receivers, or rely on deterministic DRL architectures such as deep deterministic policy gradient (DDPG), which are sensitive to value overestimation and training instability

[11]. Moreover, robust secure SWIPT designs for UAV–RIS systems typically assume PCSI or optimize RIS configuration and UAV mobility separately [5], [10]. As a result, joint worst-case SEE (WCSEE) optimization in the presence of UEHRs, imperfect CSI (ICSI), discrete RIS phase shifts, and UAV mobility remains largely unexplored.

Motivated by this gap, we study a secure downlink multiuser multiple-input single-output (MISO) system in which a multi-antenna base station (BS) serves multiple information-harvesting receivers (IHRs) in the presence of non-colluding UEHRs. A UAV-mounted RIS assists transmission via passive beamforming and mobility, while zero-forcing (ZF) precoding is employed at the BS to mitigate multiuser interference. The CSI of UEHRs is modeled by a norm-bounded uncertainty set, leading to a WCSEE maximization problem subject to transmit power, EH, and mobility constraints.

Under the joint consideration of ICSI, discrete RIS phases, and UAV mobility, the resulting WCSEE maximization problem becomes highly nonconvex due to strong channel-geometry coupling and worst-case robustness requirements. Classical optimization methods are therefore inefficient and sensitive to initialization. To address these challenges, we develop a soft actor–critic (SAC)-based DRL framework that jointly optimizes UAV horizontal positioning, RIS phase shifts, and ZF power allocation. Owing to entropy-regularized policy updates and a twin-critic architecture, the proposed SAC approach exhibits enhanced robustness to CSI uncertainty and more stable training behavior than deterministic DRL methods such as DDPG.

In addition, as a structured benchmark, we derive a novel successive convex approximation (SCA) framework based on a block coordinate descent (BCD) strategy for a simplified ideal scenario with PCSI and continuous RIS phase shifts. This SCA–BCD solution provides analytical insight and serves as a reference for evaluating the proposed SAC-based design. The main contributions of this work are summarized as follows:

- We propose a secure UAV–RIS-assisted multiuser MISO framework with SWIPT, where UEHRs may eavesdrop while harvesting energy.
- We model ICSI of UEHRs via a norm-bounded uncertainty set and derive a WCSEE formulation under EH and power constraints.
- We develop a robust SAC-based DRL solution that simultaneously optimizes UAV positioning, RIS phase control, and ZF power allocation while satisfying minimum EH requirements.
- For benchmarking purposes, we derive a tailored SCA-based optimization framework for the PCSI case with continuous RIS phase shifts.
- Extensive simulations demonstrate that the proposed SAC approach consistently outperforms SCA and DDPG benchmarks and exhibits strong robustness against CSI uncertainty, transmit power variations, and system configuration changes.

The remainder of this paper is organized as follows. Section II introduces the system and channel models and formulates the SEE maximization problem. Section III presents the proposed SAC-based solution, while Section IV details

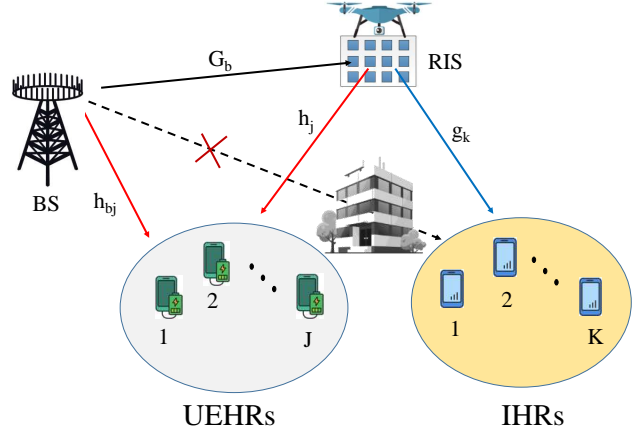


Fig. 1. System model of the UAV-assisted RIS-aided secure downlink network.

the SCA-based benchmark. Numerical results are provided in Section V, and conclusions are drawn in Section VI.

Notation: We use bold lowercase/uppercase letters for vectors/matrices. The notation $(\cdot)^T$ and $(\cdot)^H$ denote the transpose operator and the conjugate transpose operator, respectively. \Re and \Im represent the real and the imaginary parts of a complex variable, respectively. Notation \triangleq denotes a definition, while $\mathbb{R}^{N \times N}$ and $\mathbb{C}^{N \times N}$ denote the sets of $M \times N$ real and complex matrices, respectively. The matrix \mathbf{I}_N denotes the $N \times N$ identity matrix, $[\mathbf{x}]_m$ is the m -th element of a vector \mathbf{x} and $[\mathbf{X}]_{m,n}$ is the (m,n) -th element of a matrix \mathbf{X} . The operator $\text{diag}\{\cdot\}$ constructs a diagonal matrix from its vector argument.

II. SYSTEM MODEL AND PROBLEM FORMULATION

Consider a downlink wireless communication system consisting of one UAV-assisted RIS, J non-colluding UEHRs, K legitimate users, and one BS. The set of K IHRs and J UEHRs are denoted by $\mathcal{K} = \{1, \dots, K\}$ and $\mathcal{J} = \{1, \dots, J\}$, respectively. Due to the presence of high obstacles, there exists no line-of-sight (LoS) channel between the BS and the IHRs. The UAV, equipped with a RIS, serves as a passive relay to assist communication between the BS and the users. The RIS is composed of M reflecting elements, and the phase shift of each element can be controlled by the UAV. The BS is equipped with N_t antennas.

All UEHRs, IHRs, and the BS are located on the ground. The horizontal coordinates of user $k \in \mathcal{K}$, UEHR $j \in \mathcal{J}$, and the BS are denoted by $\mathbf{w}_k^I = [x_k^I, y_k^I]^T$, $\mathbf{w}_j^U = [x_j^U, y_j^U]^T$, and $\mathbf{w}_b = [x_b, y_b]^T$, respectively. The UAV-mounted RIS flies at a fixed altitude H and hovers to enhance communication. The system model is illustrated in Fig. 1.

The UAV (RIS) horizontal coordinate is denoted by $\mathbf{q} = [x_r, y_r]^T$. To capture realistic flight restrictions, the UAV is constrained to hover inside a given rectangular region

$$\mathcal{L} \triangleq \{\mathbf{q} = [x_r, y_r]^T \mid x_{\min}^r \leq x_r \leq x_{\max}^r, y_{\min}^r \leq y_r \leq y_{\max}^r\}. \quad (1)$$

Thus, the UAV location must satisfy $\mathbf{q} \in \mathcal{L}$.

A. Channel Model

Let d_b denote the distance between the BS and the UAV, and d_k and d_j denote the distances between the UAV and user k and UEHR j , respectively, i.e.,

$$d_b = \sqrt{\|\mathbf{q} - \mathbf{w}_b\|^2 + H^2}, \quad (2)$$

$$d_k = \sqrt{\|\mathbf{q} - \mathbf{w}_k^I\|^2 + H^2}, \quad k \in \mathcal{K}, \quad (3)$$

$$d_j = \sqrt{\|\mathbf{q} - \mathbf{w}_j^U\|^2 + H^2}, \quad j \in \mathcal{J}. \quad (4)$$

We adopt a distance-dependent path-loss model with exponent $\alpha \geq 2$ and a Rician small-scale fading model for all air-to-ground links. Specifically, the channel between the UAV-mounted RIS and user k is given by $\mathbf{g}_k = \sqrt{\rho_0 d_k^{-\alpha}} \tilde{\mathbf{g}}_k$, and

$$\tilde{\mathbf{g}}_k = \sqrt{\frac{K_k}{K_k + 1}} \mathbf{g}_k^{\text{LoS}} + \sqrt{\frac{1}{K_k + 1}} \hat{\mathbf{g}}_k, \quad (5)$$

where ρ_0 is the path loss at the reference distance of 1 meter, $\hat{\mathbf{g}}_k \sim \mathcal{CN}(\mathbf{0}, \mathbf{I}_M)$, and K_k is the Rician K -factor. Similarly, the UAV-UEHR j channel is $\mathbf{h}_j = \sqrt{\rho_0 d_j^{-\alpha}} \tilde{\mathbf{h}}_j$, and

$$\tilde{\mathbf{h}}_j = \sqrt{\frac{K_j}{K_j + 1}} \mathbf{h}_j^{\text{LoS}} + \sqrt{\frac{1}{K_j + 1}} \hat{\mathbf{h}}_j, \quad (6)$$

where $\hat{\mathbf{h}}_j \sim \mathcal{CN}(\mathbf{0}, \mathbf{I}_M)$ and K_j is the Rician factor.

The LoS components $\mathbf{g}_k^{\text{LoS}}$ and $\mathbf{h}_j^{\text{LoS}}$ are modeled via the RIS array steering vector. Assuming a uniform linear array (ULA) with inter-element spacing $\chi = \lambda/2$, where λ is the carrier wavelength, the steering vector of the RIS towards angle φ is

$$\mathbf{a}_{\text{RIS}}(\varphi) = [1, e^{-j\frac{2\pi}{\lambda}\chi \sin \varphi}, \dots, e^{-j\frac{2\pi}{\lambda}\chi(M-1) \sin \varphi}]^T. \quad (7)$$

It is assumed that the RIS forms a ULA parallel to the ground, so that the angular dependence of the array response is captured through the horizontal azimuth angle φ , while the UAV altitude H only affects the large-scale path loss via the 3D distance. Hence, $\mathbf{g}_k^{\text{LoS}} = \mathbf{a}_{\text{RIS}}(\varphi_k)$ and $\mathbf{h}_j^{\text{LoS}} = \mathbf{a}_{\text{RIS}}(\varphi_j)$, where φ_k and φ_j are the angles of departure from the RIS towards user k and UEHR j , respectively, determined by $\varphi_k = \arctan\left(\frac{y_k - y_r}{x_k - x_r}\right)$ and $\varphi_j = \arctan\left(\frac{y_j - y_r}{x_j - x_r}\right)$.

We define the RIS phase shift vector as $\mathbf{s} = [s_1, \dots, s_M]^T$, where each element is given by $s_m = e^{j\theta_m}$ for all $m \in \{1, \dots, M\}$. The RIS reflection-coefficient matrix is

$$\Theta = \text{diag}(s_1, \dots, s_M) \in \mathbb{C}^{M \times M}, \quad (8)$$

In the ideal continuous-phase model, the phase shift satisfies $\theta_m \in [0, 2\pi)$. In practical implementations with finite-resolution phase shifters, θ_m is restricted to a discrete set

$$\theta_m \in \mathcal{F} \triangleq \left\{0, \frac{2\pi}{2^L}, \frac{2\pi \cdot 2}{2^L}, \dots, \frac{2\pi(2^L - 1)}{2^L}\right\}, \quad (9)$$

where L denotes the number of quantization bits of each RIS element.

The channel matrix between the BS and the RIS is denoted by $\mathbf{G}_b \in \mathbb{C}^{M \times N_t}$, where $[\mathbf{G}_b]_{m,n}$ represents the channel coefficient between the n th transmit antenna at the BS and

the m th reflecting element of the RIS. It is modeled as $\mathbf{G}_b = \sqrt{\rho_0 d_b^{-\alpha}} \tilde{\mathbf{G}}_b$, and

$$\tilde{\mathbf{G}}_b = \left(\sqrt{\frac{K_b}{K_b + 1}} \mathbf{G}_b^{\text{LoS}} + \sqrt{\frac{1}{K_b + 1}} \hat{\mathbf{G}}_b \right) \quad (10)$$

where $\hat{\mathbf{G}}_b \sim \mathcal{CN}(\mathbf{0}, \mathbf{I}_{M \times N_t})$ and K_b is the Rician K -factor. The LoS component is given by

$$\mathbf{G}_b^{\text{LoS}} = \mathbf{a}_{\text{RIS}}(\varphi_{BR}) \mathbf{a}_{\text{BS}}^H(\varphi_{BR}), \quad (11)$$

with $\mathbf{a}_{\text{BS}}(\cdot)$ denoting the BS array response.

As a worst-case assumption for secrecy analysis, we also consider a direct link between the BS and each UEHR. The corresponding channel vector between the BS and the j -th UEHR is denoted by $\mathbf{h}_{bj} \in \mathbb{C}^{N_t \times 1}$ for all $j \in \mathcal{J}$, where the small-scale fading follows a Rayleigh model with

$$\mathbf{h}_{bj} \sim \mathcal{CN}(\mathbf{0}, \rho_0 d_{bj}^{-\alpha} \mathbf{I}_{N_t}), \quad (12)$$

and $d_{bj} = \|\mathbf{w}_b - \mathbf{w}_j^U\|$ is the BS-UEHR distance. For simplicity, we assume a common path loss exponent for all air-to-ground links, i.e., $\alpha_b = \alpha_k = \alpha_j = \alpha_{\text{air}} = \alpha$.

B. Signal Model and ZF Beamforming

The BS employs linear ZF precoding to simultaneously serve K IHRs. Let

$$\mathbf{H}_c = [\mathbf{h}_{c,1}, \dots, \mathbf{h}_{c,K}] \in \mathbb{C}^{N_t \times K}$$

denote the combined channel matrix of BS-RIS-IHR, where

$$\mathbf{h}_{c,k} = \mathbf{G}_b^H \Theta^H \mathbf{g}_k, \quad k \in \mathcal{K}. \quad (13)$$

The unnormalized ZF precoding matrix is obtained from the Moore-Penrose pseudo-inverse as

$$\bar{\mathbf{P}} = \mathbf{H}_c (\mathbf{H}_c^H \mathbf{H}_c)^{-1}. \quad (14)$$

The k -th column $\bar{\mathbf{p}}_k$ of $\bar{\mathbf{P}}$ satisfies $\mathbf{h}_{c,i}^H \bar{\mathbf{p}}_k = 0$ for all $i \neq k$. To incorporate transmit power allocation, each ZF precoder is normalized and scaled as

$$\mathbf{p}_k = \sqrt{\tilde{p}_k} \hat{\mathbf{p}}_k, \quad k = 1, \dots, K, \quad (15)$$

where $\tilde{p}_k \geq 0$ is the transmit power allocated to user k and $\hat{\mathbf{p}}_k$ is the corresponding normalized ZF beam direction defined as

$$\hat{\mathbf{p}}_k \triangleq \frac{\bar{\mathbf{p}}_k}{\|\bar{\mathbf{p}}_k\|}, \quad k = 1, \dots, K. \quad (16)$$

The transmitted signal from the BS is therefore

$$\mathbf{x} = \sum_{k=1}^K \mathbf{p}_k \tilde{s}_k, \quad (17)$$

where \tilde{s}_k is a unit-power information symbol intended for IHR k . Using (17), the received baseband signal at IHR k is

$$y_k = \mathbf{h}_{c,k}^H \mathbf{x} + n_k, \quad (18)$$

where $n_k \sim \mathcal{CN}(0, \sigma^2)$ is the AWGN. Following the ZF property that $\mathbf{h}_{c,k}^H \hat{\mathbf{p}}_l = 0$ for all $\ell \neq k$, the SINR at the legitimate user k , obtained as

$$\gamma_k = \frac{|\mathbf{h}_{c,k}^H \mathbf{p}_k|^2}{\sum_{\ell \neq k} |\mathbf{h}_{c,k}^H \mathbf{p}_\ell|^2 + \sigma^2} = \frac{\tilde{p}_k a_k}{\sigma^2}. \quad (19)$$

where $a_k \triangleq |\mathbf{h}_{c,k}^H \hat{\mathbf{p}}_k|^2$. The received signal at UEHR j is

$$y_j = (\mathbf{h}_{b,j}^H + \mathbf{h}_j^H \Theta \mathbf{G}_b) \mathbf{x} + n_j. \quad (20)$$

For simplicity of notations we define $\mathbf{u}_j \triangleq \mathbf{h}_{b,j} + \mathbf{G}_b^H \Theta^H \mathbf{h}_j$. Then the eavesdropping SINR for decoding user k is

$$\gamma_{j,k} = \frac{|\mathbf{u}_j^H \mathbf{p}_k|^2}{\sum_{\ell \neq k} |\mathbf{u}_j^H \mathbf{p}_\ell|^2 + \sigma^2} = \frac{\tilde{p}_k b_{j,k}}{\sum_{\ell \neq k} \tilde{p}_\ell b_{j,\ell} + \sigma^2}, \quad (21)$$

where $b_{j,k} \triangleq |\mathbf{u}_j^H \hat{\mathbf{p}}_k|^2$.

C. Worst-Case Secrecy Rate Under CSI Uncertainty

The BS is assumed to possess PCSI for the legitimate IHR links, which is reasonable due to their regular communication and feedback reporting. In contrast, UEHRs do not engage in continuous or reliable channel reporting. Their CSI is therefore *partially outdated* and only imperfect estimates are available at the BS.

To capture this inaccuracy, we adopt the widely used norm-bounded CSI uncertainty model [16], [17]. Let $\hat{\mathbf{u}}_j \in \mathbb{C}^{N_t \times 1}$ denote the estimated cascaded BS–RIS–UEHR channel for UEHR j , and let \mathbf{u}_j be the true (unknown) channel. The ICSI model is

$$\mathbf{u}_j = \hat{\mathbf{u}}_j + \Delta \mathbf{u}_j, \quad \Delta \mathbf{u}_j \in \mathcal{U}, \quad (22)$$

where the uncertainty set is

$$\mathcal{U} \triangleq \left\{ \Delta \mathbf{u}_j \in \mathbb{C}^{N_t \times 1} : \|\Delta \mathbf{u}_j\|_2 \leq \nu \right\}. \quad (23)$$

Here, $\nu > 0$ defines the radius of the CSI error region and reflects the UEHR's infrequent or unreliable feedback. When $\nu = 0$, the BS has perfect knowledge of the UEHR channel. This norm-bounded uncertainty model enables a worst-case secrecy formulation, ensuring robustness against the strongest possible UEHR eavesdropping behavior within the uncertainty region.

Since \mathbf{u}_j is imperfectly known, the BS must ensure robustness against the *worst-case eavesdropping capability* within the uncertainty region. To account for channel uncertainty, we adopt standard norm-bounded channel uncertainty results. For any channel model $\mathbf{h} = \hat{\mathbf{h}} + \Delta \mathbf{h}$ with $\|\Delta \mathbf{h}\|_2 \leq \nu$ and for any vector $\mathbf{p} \in \mathbb{C}^n$, the following bounds hold (see [8], [18])

$$\max_{\|\Delta \mathbf{h}\|_2 \leq \nu} |\mathbf{h}^H \mathbf{p}| = |\hat{\mathbf{h}}^H \mathbf{p}| + \nu \|\mathbf{p}\|_2, \quad (24a)$$

$$\min_{\|\Delta \mathbf{h}\|_2 \leq \nu} |\mathbf{h}^H \mathbf{p}| = \left[|\hat{\mathbf{h}}^H \mathbf{p}| - \nu \|\mathbf{p}\|_2 \right]^+, \quad (24b)$$

where $[x]^+ = \max(x, 0)$. Applying (24) to the numerator and denominator terms of the eavesdropping SINR in (21) yields

$$\max_{\|\Delta \mathbf{u}_j\|_2 \leq \nu} |\mathbf{u}_j^H \mathbf{p}_k|^2 = \left(|\hat{\mathbf{u}}_j^H \mathbf{p}_k| + \nu \|\mathbf{p}_k\| \right)^2, \quad (25)$$

$$\min_{\|\Delta \mathbf{u}_j\|_2 \leq \nu} |\mathbf{u}_j^H \mathbf{p}_\ell|^2 = \left([|\hat{\mathbf{u}}_j^H \mathbf{p}_\ell| - \nu \|\mathbf{p}_\ell\|]^+ \right)^2, \quad \ell \neq k. \quad (26)$$

Accordingly, a conservative upper bound on the worst-case eavesdropping SINR for user k at UEHR j is obtained as

$$\begin{aligned} \gamma_{E,k} &= \max_{j \in \mathcal{J}} \left\{ \max_{\|\Delta \mathbf{u}_j\|_2 \leq \nu} \hat{\gamma}_{j,k}(\Delta \mathbf{u}_j) \right\} \\ &\leq \max_{j \in \mathcal{J}} \frac{\left(|\hat{\mathbf{u}}_j^H \mathbf{p}_k| + \nu \|\mathbf{p}_k\| \right)^2}{\sum_{\ell \neq k} \left([|\hat{\mathbf{u}}_j^H \mathbf{p}_\ell| - \nu \|\mathbf{p}_\ell\|]^+ \right)^2 + \sigma^2} \\ &= \max_{j \in \mathcal{J}} \frac{\tilde{p}_k \left(\sqrt{\hat{b}_{j,k}} + \nu \right)^2}{\sum_{\ell \neq k} \tilde{p}_\ell \left(\left[\sqrt{\hat{b}_{j,\ell}} - \nu \right]^+ \right)^2 + \sigma^2}, \end{aligned} \quad (27)$$

where $\hat{b}_{j,k} \triangleq |\hat{\mathbf{u}}_j^H \hat{\mathbf{p}}_k|^2$, $\forall j \in \mathcal{J}$, $k \in \mathcal{K}$. Given the legitimate-user SINR γ_k and the upper bound on the worst-case eavesdropping SINR $\gamma_{E,k}$ in (27), the worst-case secrecy rate of IHR k is expressed as

$$R_k^{\text{sec}} = \left[\log_2(1 + \gamma_k) - \log_2(1 + \gamma_{E,k}) \right]^+. \quad (28)$$

This formulation guarantees secrecy robustness against all UEHR channel realizations satisfying $\|\Delta \mathbf{u}_j\| \leq \nu$.

The total received RF power at UEHR j is

$$P_j^{\text{EH}} = \sum_{k=1}^K |\mathbf{u}_j^H \mathbf{p}_k|^2, \quad (29)$$

and the harvested DC power follows the logistic nonlinear model [19]

$$\Omega(P_j^{\text{EH}}) = \frac{b_2}{k'_1 (1 + \exp(-b_0(P_j^{\text{EH}} - b_1)))} - k'_2. \quad (30)$$

where $\Omega(\cdot)$ is a logistic function representing the non-linear energy harvesting model, and k'_1 , k'_2 , b_0 , b_1 , b_2 are positive constants. The required EH power must satisfy the following constraint

$$\sum_{j \in \mathcal{J}} \min_{\|\Delta \mathbf{u}_j\|_2 \leq \nu} P_j^{\text{EH}} \geq \Omega^{-1}(E_h), \quad (31)$$

where E_h denotes the minimum harvested energy requirement at the set of UEHRs. The inverse function $\Omega^{-1}(x)$ is defined as

$$\Omega^{-1}(x) = b_1 - \frac{1}{b_0} \ln \left(\frac{b_2}{k'_1 (x + k'_2)} - 1 \right). \quad (32)$$

To obtain a tractable deterministic formulation, (31) is enforced via the following sufficient lower-bound constraint

$$\sum_{j \in \mathcal{J}} \underline{P}_j^{\text{EH}} \geq \Omega^{-1}(E_h), \quad (33)$$

where

$$\underline{P}_j^{\text{EH}} \triangleq \sum_{k=1}^K \left([|\hat{\mathbf{u}}_j^H \mathbf{p}_k| - \nu \|\mathbf{p}_k\|_2]^+ \right)^2, \quad \forall j \in \mathcal{J}. \quad (34)$$

D. Problem Formulation

To guarantee confidentiality against UEHRs, the secrecy rate of each legitimate IHR is defined under worst-case eavesdropping as in (28). To ensure fairness among users, we adopt the minimum secrecy rate

$$R^{\sec} = \min_{k \in \mathcal{K}} R_k^{\sec}. \quad (35)$$

We aim to maximize the WCSEE, defined as the ratio between the minimum secrecy rate and the total power consumption at the BS. The total power includes the radiated transmit power and the circuit power consumption. The optimization variables include the ZF power allocation, RIS phase shifts, and the UAV horizontal position. The resulting problem is formulated as

$$\max_{\tilde{\mathbf{p}}, \boldsymbol{\theta}, \mathbf{q}} \frac{R^{\sec}}{\varrho \sum_{k=1}^K \tilde{p}_k + P_0} \quad (36a)$$

$$\text{s.t. } \sum_{k=1}^K \tilde{p}_k \leq P_{\max}, \quad (36b)$$

$$\theta_m \in \mathcal{F}, \quad m = 1, \dots, M, \quad (36c)$$

$$\mathbf{q} \in \mathcal{L}, \quad (36d)$$

$$(33). \quad (36e)$$

where ϱ is the reciprocal of the drain efficiency of the power amplifier at the BS [20], $\tilde{\mathbf{p}} = \{\tilde{p}_k\}_{k=1}^K$, $\boldsymbol{\theta} = \{\theta_m\}_{m=1}^M$ and P_0 represents the circuit power consumption.

Remark 1. Problem (36) is highly nonconvex due to the fractional SEE objective, the coupled channel-geometry dependence, the worst-case secrecy constraints, and the discrete RIS phase shifts. This motivates the use of DRL-based methods, which can directly handle the resulting high-dimensional nonconvex optimization.

III. SAC-BASED JOINT ZF POWER ALLOCATION, RIS PHASE, AND LOCATION OPTIMIZATION

The WCSEE maximization problem formulated in Section II-D is highly nonconvex due to (i) the fractional SEE objective, (ii) the coupled channel-geometry dependence induced by the UAV-mounted RIS, (iii) the worst-case secrecy constraints under UEHR CSI uncertainty, and (iv) the discrete RIS phase shifts imposed by practical hardware. Thus, conventional alternating optimization or SCA techniques suffer from poor scalability and are prone to local optima.

To overcome these limitations, we adopt a SAC framework that learns optimal control policies directly through interaction with the wireless environment. SAC naturally handles high-dimensional continuous action spaces, provides stable learning via entropy regularization, and accommodates discrete RIS phase constraints through continuous relaxation and projection, making it particularly suitable for the proposed robust UAV-RIS optimization problem. In the following subsections, the joint optimization problem is first formulated as a Markov decision process (MDP), after which a SAC algorithm is employed to obtain the solution.

A. MDP Model

The joint optimization problem is modeled as a MDP characterized by the tuple $\langle \mathcal{S}, \mathcal{A}, \mathcal{P}, \mathcal{R} \rangle$. At each decision step t , the agent observes the system state $s_t \in \mathcal{S}$, selects an action $a_t \in \mathcal{A}$ according to a stochastic policy $\pi(a_t | s_t)$, and receives an instantaneous reward $r_t = \mathcal{R}(s_t, a_t)$. The components of the MDP are defined as follows.

- Action: The action consists of the control variables to be optimized, namely the ZF power allocation, RIS phase shifts, and UAV horizontal position

$$a_t = [\{\tilde{p}_k^{(t)}\}_{k=1}^K, \{\theta_m^{(t)}\}_{m=1}^M, \mathbf{q}^{(t)}]. \quad (37)$$

The SAC agent outputs a continuous action vector in $[-1, 1]^{K+M+2}$ by employing a \tanh activation function at the output layer of the actor network, which is then mapped to the physical control variables as follows. The elements corresponding to power allocation are first mapped to $\hat{p}_k^{(t)} \in [0, 1]$ via affine scaling. To strictly satisfy the transmit power constraint in (36b), the power allocation is normalized as

$$\tilde{p}_k^{(t)} = P_{\max} \frac{\hat{p}_k^{(t)}}{\sum_{\ell=1}^K \hat{p}_\ell^{(t)}}, \quad \forall k \in \mathcal{K}, \quad (38)$$

with $\sum_{\ell=1}^K \hat{p}_\ell^{(t)} > 0$; otherwise $\tilde{p}_k^{(t)} = 0$. The RIS phase variables are mapped as $\theta_m^{(t)} \in [0, 2\pi)$ and then quantized to the nearest feasible value in \mathcal{F} , while the UAV horizontal position $\mathbf{q}^{(t)}$ is projected onto the feasible region \mathcal{L} .

- State: The state captures the channel and geometric information relevant to secrecy-aware transmission:

$$s_t = [\Re\{\mathbf{H}_c\}, \Im\{\mathbf{H}_c\}, \Re\{\hat{\mathbf{u}}_j\}_{j=1}^J, \Im\{\hat{\mathbf{u}}_j\}_{j=1}^J, x_r^{(t)}, y_r^{(t)}], \quad (39)$$

Within each episode, user and UEHR locations remain fixed, whereas new realizations are drawn across episodes.

- Reward: Given the action a_t , the ZF precoder is constructed and scaled according to $\{\tilde{p}_k^{(t)}\}$, and the worst-case eavesdropping SINR $\gamma_{E,k}^{(t)}$ is evaluated using the closed-form bound derived in (27). The total power consumption is

$$P_{\text{tot}}^{(t)} = \varrho \sum_{k=1}^K \tilde{p}_k^{(t)} + P_0. \quad (40)$$

Accordingly, the instantaneous reward is defined as

$$r_t = \begin{cases} \frac{R^{\sec, (t)}}{P_{\text{tot}}^{(t)}}, & \text{if (33) holds,} \\ 0, & \text{otherwise,} \end{cases} \quad (41)$$

where $R^{\sec, (t)}$ denotes the minimum secrecy rate defined in (35) evaluated at step t .

B. Fundamentals of the SAC Algorithm

Unlike conventional DRL algorithms that only maximize the expected cumulative reward, the SAC algorithm augments the objective with an entropy term to encourage policy exploration and improve training stability. The optimal policy π^* is obtained by solving the maximum-entropy RL problem [21]:

$$\pi^* = \arg \max_{\pi} \mathbb{E}_{(s_t, a_t) \sim \rho_{\pi}} \left[\sum_{t=0}^{\infty} (r_t + \beta \mathcal{H}(\pi(\cdot|s_t))) \right], \quad (42)$$

where ρ_{π} denotes the state-action visitation distribution under policy π , $\mathcal{H}(\pi(\cdot|s_t)) \triangleq -\mathbb{E}_{a_t \sim \pi(\cdot|s_t)} [\log \pi(a_t|s_t)]$ denotes the policy entropy, and $\beta > 0$ is the temperature parameter that balances exploitation and exploration.

In SAC, two soft Q-functions $Q_{\phi_1}(s, a)$ and $Q_{\phi_2}(s, a)$, parameterized by neural networks with parameters ϕ_1 and ϕ_2 , are employed to approximate the soft state-action value:

$$Q^{\pi}(s_t, a_t) = \mathbb{E}[r_t + \gamma V^{\pi}(s_{t+1})], \quad (43)$$

where $\gamma \in [0, 1]$ is the discount factor weighting future and instant rewards and the soft value function is given by

$$V^{\pi}(s_{t+1}) = \mathbb{E}_{a_{t+1} \sim \pi}[Q^{\pi}(s_{t+1}, a_{t+1}) - \beta \log \pi(a_{t+1}|s_{t+1})]. \quad (44)$$

In practice, the soft value function is not explicitly parameterized and is instead evaluated implicitly using the current policy and target Q-networks, in accordance with the modern SAC formulation. Given a replay buffer \mathcal{D} containing transition tuples (s_t, a_t, r_t, s_{t+1}) , the critic networks are trained by minimizing the following mean-squared soft Bellman error

$$J_Q(\phi_i) = \mathbb{E}_{(s_t, a_t, r_t, s_{t+1}) \sim \mathcal{D}} \left[\frac{1}{2} \left(Q_{\phi_i}(s_t, a_t) - y_t \right)^2 \right], \quad (45)$$

where $i \in \{1, 2\}$ and

$$y_t = r_t + \gamma \mathbb{E}_{a_{t+1} \sim \pi(\cdot|s_{t+1})} \left[\min_{j=1,2} Q_{\bar{\phi}_j}(s_{t+1}, a_{t+1}) - \beta \log \pi(a_{t+1}|s_{t+1}) \right], \quad (46)$$

with $\bar{\phi}_j$ denoting the parameters of the corresponding target Q-networks.

The actor (policy) network $\pi_{\psi}(a|s)$, parameterized by ψ , is updated by minimizing

$$J_{\pi}(\psi) = \mathbb{E}_{s_t \sim \mathcal{D}} \left[\mathbb{E}_{a_t \sim \pi_{\psi}} \left(\beta \log \pi_{\psi}(a_t|s_t) - \min_{i=1,2} Q_{\phi_i}(s_t, a_t) \right) \right]. \quad (47)$$

The temperature β is tuned automatically by minimizing [22]

$$J(\beta) = \mathbb{E}_{(s_t, a_t) \sim \mathcal{D}} \left[-\beta (\log \pi_{\psi}(a_t|s_t) + \bar{\mathcal{H}}) \right], \quad (48)$$

where $\bar{\mathcal{H}}$ is a target entropy level, typically set as a negative constant proportional to the action dimension.

Beyond this practical perspective, SAC admits a useful interpretation based on probabilistic inference: the policy

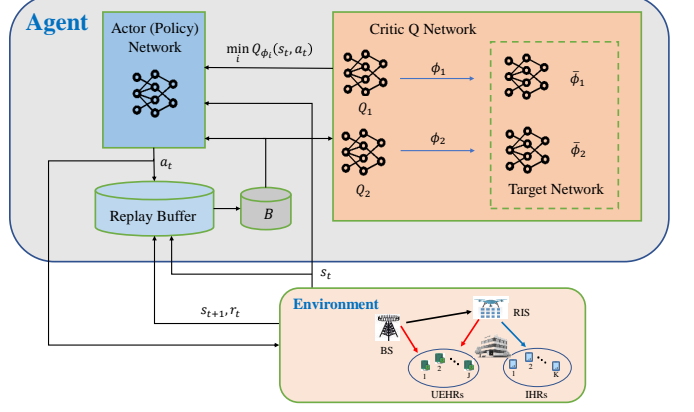


Fig. 2. SAC framework for joint power allocation, RIS phase optimization, and UAV positioning with twin critics and target Q-networks.

improvement step corresponds to projecting the policy distribution toward an energy-based target distribution. Formally, the optimal policy solves

$$J_{\pi}(\psi) = \mathbb{E}_{s_t \sim \mathcal{D}} \left[D_{\text{KL}} \left(\pi_{\psi}(\cdot|s_t) \parallel \frac{\exp(Q_{\theta}(s_t, \cdot)/\beta)}{Z_{\theta}(s_t)} \right) \right], \quad (49)$$

where $D_{\text{KL}}(\cdot \parallel \cdot)$ denotes the Kullback–Leibler divergence and $Z_{\theta}(s_t)$ is a normalizing partition function. This viewpoint reveals that SAC implicitly projects the policy toward a Boltzmann distribution induced by the critic values, which explains its stable convergence and robust exploration behaviour.

C. SAC-Based Joint Optimization Framework

Unlike deterministic actor–critic baselines, SAC updates the policy via an entropy-regularized objective without a target actor network. Fig. 2 depicts the interaction between the SAC agent and the wireless environment. At each step, the agent observes the state s_t and samples a continuous action $a_t \sim \pi_{\psi}(\cdot|s_t)$ that jointly controls the power allocation, RIS phase-shift vector, and UAV horizontal position. The critic employs twin Q-networks Q_{ϕ_1} and Q_{ϕ_2} , and the minimum Q-value is used to mitigate overestimation bias. Target critic networks $\{Q_{\bar{\phi}_1}, Q_{\bar{\phi}_2}\}$ are updated via Polyak averaging to stabilize Bellman backups, while the entropy temperature β is automatically tuned to match a target entropy level. The environment maps actions to feasible variables via power normalization, RIS phase quantization, and location projection, and returns the reward based on the hard energy-harvesting constraint and the resulting WCSEE. Transitions are stored in a replay buffer and mini-batches are sampled to update the actor, critics, and β as summarized in Algorithm 1. After training, π_{ψ} enables real-time joint control under different channel realizations and network geometries.

IV. SCA-BASED SOLUTION

The WCSEE maximization problem in (36) is highly non-convex due to the fractional objective function, the coupled UAV–RIS channel geometry, the discrete RIS phase constraints, and the presence of UEHR CSI uncertainty. Although

Algorithm 1: SAC-Based Joint Power Allocation, RIS Phase and Location Optimization

Input : Discount factor γ , learning rates $\lambda_Q, \lambda_\pi, \lambda_\beta$, target entropy \bar{H} , soft update coefficient τ , batch size B .

Output: Stochastic policy $\pi_\psi(a|s)$.

- 1 Initialize replay buffer \mathcal{D} .
- 2 Initialize critics Q_{ϕ_1}, Q_{ϕ_2} and target critics $Q_{\bar{\phi}_1}, Q_{\bar{\phi}_2}$ with $\bar{\phi}_i \leftarrow \phi_i$.
- 3 Initialize policy network π_ψ and temperature β .
- 4 **for** each training episode **do**
- 5 Reset environment and observe initial state s_0 .
- 6 **for** each time step t **do**
- 7 Observe state s_t and sample action $a_t \sim \pi_\psi(\cdot|s_t)$.
- 8 Map a_t to $\{\tilde{p}_k^{(t)}\}$, $\{\phi_m^{(t)}\}$, and $\mathbf{q}^{(t)}$, execute in environment, and obtain (r_t, s_{t+1}) .
- 9 Store (s_t, a_t, r_t, s_{t+1}) in replay buffer \mathcal{D} .
- 10 **for** each gradient update **do**
- 11 Sample mini-batch $\{(s_t, a_t, r_t, s_{t+1})\}$ from \mathcal{D} .
- 12 Update critics with (45)
- 13 $\phi_i \leftarrow \phi_i - \lambda_Q \nabla_{\phi_i} J_Q(\phi_i)$, $i = 1, 2$.
- 14 Update policy with (47) $\psi \leftarrow \psi - \lambda_\pi \nabla_\psi J_\pi(\psi)$.
- 15 Update temperature with (48) $\beta \leftarrow \beta - \lambda_\beta \nabla_\beta J(\beta)$.
- 16 Update target critics $\bar{\phi}_i \leftarrow \tau \phi_i + (1 - \tau) \bar{\phi}_i$, $i = 1, 2$.

the proposed SAC-based solution is designed to directly address these challenges, it is instructive to develop a model-based benchmark under idealized assumptions to validate the effectiveness of the proposed learning framework.

Specifically, in this section we consider an ideal reference case with PCSI for all links and continuous RIS phase shifts. Under these assumptions, problem (36) admits a tractable approximation that can be efficiently solved via SCA. Accordingly, under the above idealized assumptions, problem (36) reduces to

$$\max_{\tilde{\mathbf{p}}, \boldsymbol{\theta}, \mathbf{q}} \frac{R^{\text{sec}}}{\varrho \sum_{k=1}^K \tilde{p}_k + P_0} \quad (50a)$$

$$\text{s.t. } \sum_{j \in \mathcal{J}} P_j^{\text{EH}} \geq \Omega^{-1}(E_h), \quad (50b)$$

$$\theta_m \in [0, 2\pi], \quad \forall m \in \{1, \dots, M\}, \quad (50c)$$

$$(36b), (36d). \quad (50d)$$

Problem P2 is addressed using a BCD framework. Specifically, the power allocation, RIS reflection coefficients, and UAV location are optimized in an alternating manner, while the remaining variables are fixed in each subproblem.

A. Power Allocation

The RIS configuration $\boldsymbol{\Theta}$ and the UAV location \mathbf{q} are assumed fixed. Accordingly, the BS computes the ZF beamform-

ing directions from the effective channel and only optimizes the power loading.

Given fixed $\boldsymbol{\Theta}$ and \mathbf{q} , the power allocation benchmark problem is formulated as

$$\max_{\tilde{\mathbf{p}} \succeq 0} \frac{R^{\text{sec}}(\tilde{\mathbf{p}})}{\varrho \sum_{k=1}^K \tilde{p}_k + P_0} \quad (51a)$$

$$\text{s.t. } \sum_{j \in \mathcal{J}} \sum_{k=1}^K \tilde{p}_k b_{j,k} \geq \Omega^{-1}(E_h), \quad (51b)$$

$$(36b). \quad (51c)$$

In (51b), we have used (15), under which the harvested RF power at UEHR j is given by

$$P_j^{\text{EH}}(\tilde{\mathbf{p}}) = \sum_{k=1}^K \tilde{p}_k b_{j,k}. \quad (52)$$

As a result, the energy-harvesting constraint in (51b) is affine with respect to the power allocation vector $\tilde{\mathbf{p}}$.

Problem (51) is a nonlinear fractional program. Applying Dinkelbach's method [23], we introduce $\lambda \geq 0$ and the slack variable ζ to obtain the parametric form

$$\max_{\tilde{\mathbf{p}} \succeq 0, \zeta} \zeta - \lambda \left(\varrho \sum_{k=1}^K \tilde{p}_k + P_0 \right) \quad (53a)$$

$$\text{s.t. } \zeta \leq R_k^{\text{sec}}(\tilde{\mathbf{p}}), \quad \forall k \in \mathcal{K}, \quad (53b)$$

$$(36b), (51b). \quad (53c)$$

The Dinkelbach parameter is updated as

$$\lambda^{(t)} = \frac{\zeta^{(t-1)}}{\varrho \sum_{k=1}^K \tilde{p}_k^{(t-1)} + P_0}. \quad (54)$$

The secrecy constraint (53b) is nonconvex so we resort to SCA to reformulate it. To remove $\max_{j \in \mathcal{J}}$ in (27), we enforce the secrecy bound for all UEHRs

$$\zeta \leq \log_2(1 + \gamma_k) - \log_2(1 + \gamma_{j,k}), \quad \forall k \in \mathcal{K}, \forall j \in \mathcal{J}. \quad (55)$$

Using (19) and (21), we can rewrite (55) as

$$\begin{aligned} \zeta \leq & \log_2(\sigma^2 + \tilde{p}_k a_k) - \log_2(\sigma^2) + \log_2\left(\sigma^2 + \sum_{\ell \neq k} \tilde{p}_\ell b_{j,\ell}\right) \\ & - \log_2\left(\sigma^2 + \sum_{\ell=1}^K \tilde{p}_\ell b_{j,\ell}\right), \quad \forall k, \forall j. \end{aligned} \quad (56)$$

The last term in (56) is concave in $\tilde{\mathbf{p}}$ and is upper bounded by its first-order Taylor expansion at $\tilde{\mathbf{p}}^{(t)}$:

$$\log_2\left(\sigma^2 + \sum_{\ell=1}^K \tilde{p}_\ell b_{j,\ell}\right) \leq \log_2(S_j^{(t)}) + \sum_{\ell=1}^K \eta_{j,\ell}^{(t)} (\tilde{p}_\ell - \tilde{p}_\ell^{(t)}), \quad (57)$$

where $S_j^{(t)} \triangleq \sigma^2 + \sum_{\ell=1}^K \tilde{p}_\ell^{(t)} b_{j,\ell}$ and $\eta_{j,\ell}^{(t)} \triangleq \frac{b_{j,\ell}}{\ln(2) S_j^{(t)}}$. By substituting (57) into (56), we obtain the SCA lower bound:

$$\begin{aligned} \zeta \leq & \log_2(\sigma^2 + \tilde{p}_k a_k) - \log_2(\sigma^2) + \log_2\left(\sigma^2 + \sum_{\ell \neq k} \tilde{p}_\ell b_{j,\ell}\right) \\ & - \log_2(S_j^{(t)}) - \sum_{\ell=1}^K \eta_{j,\ell}^{(t)} (\tilde{p}_\ell - \tilde{p}_\ell^{(t)}), \quad \forall k \in \mathcal{K}, \forall j \in \mathcal{J}. \end{aligned} \quad (58)$$

Algorithm 2: Dinkelbach–SCA Power Allocation (Given Θ and \mathbf{q})

Input: Initial values $\zeta^{(0)}$, $\tilde{\mathbf{p}}^{(0)}$, tolerance ε , $t = 1$.

Output: Power allocation $\tilde{\mathbf{p}}^*$

- 1 **repeat**
- 2 | Update $\lambda^{(t)}$ using (54);
- 3 | Solve the convex subproblem (59);
- 4 | Set $t \leftarrow t + 1$;
- 5 **until** $|\zeta^{(t)} - \zeta^{(t-1)}| \leq \varepsilon$;
- 6 **return** $\tilde{\mathbf{p}}^{(t)}$.

At SCA iteration t (within a fixed Dinkelbach parameter $\lambda^{(t)}$), we solve

$$(\zeta^{(t)}, \tilde{\mathbf{p}}^{(t)}) = \arg \max_{\tilde{\mathbf{p}} \succeq \mathbf{0}, \zeta} \zeta - \lambda^{(t)} \left(\varrho \sum_{k=1}^K \tilde{p}_k + P_0 \right) \quad (59a)$$

$$\text{s.t. } (58), (36b), (51b). \quad (59b)$$

Problem (59) is convex and can be solved efficiently by standard solvers. At each iteration t , the SCA approximation is constructed around $\tilde{\mathbf{p}}^{(t-1)}$, and the resulting convex problem (59) is solved once using CVX. The overall Dinkelbach–SCA procedure is shown in Algorithm 2.

B. RIS Reflection Phase Optimization

In this subsection, we optimize the RIS reflection coefficients for fixed ZF beamforming directions, power allocation $\tilde{\mathbf{p}}$, and UAV location \mathbf{q} . Since the transmit power consumption at the BS is fixed under given $\tilde{\mathbf{p}}$, the WCSEE maximization reduces to a worst-case secrecy rate maximization problem. Accordingly, the RIS phase optimization subproblem can be formulated as

$$\max_{\mathbf{s}, \zeta} \zeta \quad (60a)$$

$$\text{s.t. } R_k^{\text{sec}} \geq \zeta, \quad \forall k \in \mathcal{K}, \quad (60b)$$

$$(50b), (50c). \quad (60c)$$

For any vectors $\mathbf{v} \in \mathbb{C}^M$ and $\mathbf{w} \in \mathbb{C}^{N_t}$, the cascaded channel term can be rewritten as $\mathbf{v}^H \Theta \mathbf{G}_b \mathbf{w} = \mathbf{t}^H \mathbf{s}$, where $\mathbf{t} \triangleq (\text{diag}(\mathbf{v}^H) \mathbf{G}_b \mathbf{w})^*$. Accordingly, we define

$$\mathbf{t}_{k,\ell} \triangleq (\text{diag}(\mathbf{g}_k^H) \mathbf{G}_b \mathbf{p}_\ell)^*, \quad \forall k \in \mathcal{K}, \forall \ell \in \mathcal{K}, \quad (61)$$

$$\mathbf{t}_{j,\ell} \triangleq (\text{diag}(\mathbf{h}_j^H) \mathbf{G}_b \mathbf{p}_\ell)^*, \quad \forall j \in \mathcal{J}, \forall \ell \in \mathcal{K}, \quad (62)$$

$$c_{j,\ell} \triangleq \mathbf{h}_{bj}^H \mathbf{p}_\ell, \quad \forall j \in \mathcal{J}, \forall \ell \in \mathcal{K}. \quad (63)$$

Then the useful and interference terms become

$$\mathbf{h}_{c,k}^H \mathbf{p}_\ell = \mathbf{g}_k^H \Theta \mathbf{G}_b \mathbf{p}_\ell = \mathbf{t}_{k,\ell}^H \mathbf{s}, \quad (64)$$

$$\mathbf{u}_j^H \mathbf{p}_\ell = \mathbf{h}_{bj}^H \mathbf{p}_\ell + \mathbf{h}_j^H \Theta \mathbf{G}_b \mathbf{p}_\ell = c_{j,\ell} + \mathbf{t}_{j,\ell}^H \mathbf{s}. \quad (65)$$

Using the definitions above, the received signal powers appearing in γ_k and $\gamma_{j,k}$ can be expressed as quadratic forms in \mathbf{s} . The secrecy constraint (60b) is nonconvex due to the difference of logarithmic functions. Following the SCA principle, we introduce first-order approximations of the nonconvex

quadratic terms. Introduce auxiliary variables ρ_k and $\rho_{E,j,k}$ such that

$$\rho_k \leq \gamma_k, \quad \forall k \in \mathcal{K}, \quad (66a)$$

$$\rho_{E,j,k} \geq \gamma_{j,k}, \quad \forall j \in \mathcal{J}, \forall k \in \mathcal{K}. \quad (66b)$$

Also introduce $f_{E,k}$ to handle the worst UEHR,

$$f_{E,k} \geq \log_2(1 + \rho_{E,j,k}), \quad \forall j \in \mathcal{J}, \forall k \in \mathcal{K}, \quad (67)$$

Proposition 1. An affine approximation of the secrecy-related constraints in (60b), for all $k \in \mathcal{K}$ and $j \in \mathcal{J}$, is given by

$$\sum_{\ell \neq k} |\mathbf{t}_{k,\ell}^H \mathbf{s}|^2 + \sigma^2 - \Psi^{(t)}(\mathbf{s}, \rho_k; \mathbf{t}_{kk}) \leq 0, \quad \forall k \in \mathcal{K}, \quad (68a)$$

$$|c_{j,k} + \mathbf{t}_{j,k}^H \mathbf{s}|^2 \leq \Theta^{(t)}(\xi_{j,k}, \rho_{E,j,k}), \quad \forall j \in \mathcal{J}, \forall k \in \mathcal{K}, \quad (68b)$$

$$\xi_{j,k} \leq \sum_{\ell \neq k} \vartheta^{(t)}(c_{j,\ell}, \mathbf{t}_{j,\ell}; \mathbf{s}) + \sigma^2, \quad \forall j \in \mathcal{J}, \forall k \in \mathcal{K}, \quad (68c)$$

$$1 - \Gamma^{(t)}(f_{E,k}) + \rho_{E,j,k} \leq 0, \quad \forall j \in \mathcal{J}, \forall k \in \mathcal{K}, \quad (68d)$$

$$\zeta \leq \log_2(1 + \rho_k) - f_{E,k}, \quad \forall k \in \mathcal{K}. \quad (68e)$$

where $\Psi^{(t)}(\mathbf{s}, \rho_k; \mathbf{t}_{kk})$ is the first-order Taylor approximation of $\frac{|\mathbf{t}_{kk}^H \mathbf{s}|^2}{\rho_k}$, $\Gamma^{(t)}(x) \triangleq 2^{x^{(t-1)}} [1 + \ln(2)(x - x^{(t-1)})]$ is the first-order Taylor approximation of 2^x , and

$$\begin{aligned} \Theta^{(t)}(x, y) &\triangleq \frac{1}{2}(x^{(t-1)} + y^{(t-1)})(x + y) \\ &\quad - \frac{1}{4}(x^{(t-1)} + y^{(t-1)})^2 - \frac{1}{4}(x - y)^2, \end{aligned} \quad (69)$$

is used to obtain an affine lower bound of the bilinear term xy . Moreover, $\vartheta^{(t)}(c; \mathbf{t}; \mathbf{s})$ is the first-order Taylor approximation of $|c + \mathbf{t}^H \mathbf{s}|^2$ at iteration t :

$$\vartheta^{(t)}(c; \mathbf{t}; \mathbf{s}) = 2 \Re \left\{ (\mathbf{c} + \mathbf{t}^H \mathbf{s}^{(t-1)})^H \mathbf{t}^H \mathbf{s} \right\} - |c + \mathbf{t}^H \mathbf{s}^{(t-1)}|^2. \quad (70)$$

Proof. See Appendix A. ■

Constraint (50b) is nonconvex due to the quadratic terms in \mathbf{s} , and the unit-modulus constraint $|s_m| = 1$ is also nonconvex. In the following, we construct convex surrogate constraints using SCA. Under fixed $\{\mathbf{p}_k\}$ and \mathbf{q} , the harvested RF power at UEHR j can be written as

$$P_j^{\text{EH}} = \sum_{k=1}^K |c_{j,k} + \mathbf{t}_{j,k}^H \mathbf{s}|^2. \quad (71)$$

Since $|c_{j,k} + \mathbf{t}_{j,k}^H \mathbf{s}|^2$ is convex in \mathbf{s} , its first-order Taylor expansion $\vartheta^{(t)}(c_{j,k}; \mathbf{t}_{j,k}; \mathbf{s})$ provides a global affine lower bound. Hence, an SCA-safe sufficient condition for (50b) is

$$\sum_{j \in \mathcal{J}} \sum_{k=1}^K \vartheta^{(t)}(c_{j,k}; \mathbf{t}_{j,k}; \mathbf{s}) \geq \Omega^{-1}(E_h). \quad (72)$$

In the ideal continuous-phase model, the RIS coefficients satisfy $|s_m| = 1, \forall m$. Following the penalty-based approach [24], we relax $|s_m| = 1$ to $|s_m| \leq 1$ and add a penalty term

Algorithm 3: SCA-Based RIS Phase Optimization
(Given $\tilde{\mathbf{p}}$ and \mathbf{q})

Input: Initial $\mathbf{s}^{(0)}$, tolerance $\varepsilon > 0$, penalty weight $C > 0$.

Output: Optimized RIS phase vector \mathbf{s}^* .

1 Set $t \leftarrow 1$;
2 **repeat**
3 Solve (73) to obtain $(\mathbf{s}^{(t)}, \zeta^{(t)})$;
4 $t \leftarrow t + 1$;
5 **until** $|\zeta^{(t)} - \zeta^{(t-1)}| \leq \varepsilon$;
6 **return** $\mathbf{s}^{(t-1)}$;

to encourage $|s_m|$ approaches 1. Given $\mathbf{s}^{(t-1)}$, we solve the following convex problem

$$\max_{\Xi} \zeta + C \left(2 \operatorname{Re} \left\{ (\mathbf{s}^{(t-1)})^H \mathbf{s} \right\} - \|\mathbf{s}^{(t-1)}\|^2 \right) \quad (73a)$$

$$\text{s.t. } (68a) - (68e), (72), \quad (73b)$$

$$|s_m| \leq 1, \quad \forall m = 1, \dots, M, \quad (73c)$$

where the optimization variable set is defined as $\Xi \triangleq \{\mathbf{s}, \zeta, \rho, \rho_E, \mathbf{f}_E, \xi\}$ with $\rho \triangleq \{\rho_k\}_{k \in \mathcal{K}}$, $\rho_E \triangleq \{\rho_{E,j,k}\}_{j \in \mathcal{J}, k \in \mathcal{K}}$, $\mathbf{f}_E \triangleq \{f_{E,k}\}_{k \in \mathcal{K}}$ and $\xi \triangleq \{\xi_{j,k}\}_{j \in \mathcal{J}, k \in \mathcal{K}}$. The RIS phase optimization procedure is summarized in Algorithm 3.

C. UAV Location Optimization

In this subsection, we optimize the UAV horizontal position \mathbf{q} while keeping the BS precoders $\{\mathbf{p}_k\}_{k \in \mathcal{K}}$, and the RIS phase matrix Θ fixed. Under fixed $\{\mathbf{p}_k\}$, the BS transmit power is constant; hence, the SEE maximization reduces to maximizing the minimum secrecy rate. To obtain a numerically stable and low-complexity SCA benchmark, we further consider the relaxed objective of maximizing the minimum rate of IHRs instead of the secrecy rate.

1) *Channel Separation and SINR Representation:* Using the distance definitions in (2)–(4), the channels can be expressed as

$$\mathbf{g}_k(\mathbf{q}) = \sqrt{\rho_0} d_k(\mathbf{q})^{-\frac{\alpha}{2}} \tilde{\mathbf{g}}_k, \quad \forall k \in \mathcal{K}, \quad (74)$$

$$\mathbf{h}_j(\mathbf{q}) = \sqrt{\rho_0} d_j(\mathbf{q})^{-\frac{\alpha}{2}} \tilde{\mathbf{h}}_j, \quad \forall j \in \mathcal{J}, \quad (75)$$

$$\mathbf{G}_b(\mathbf{q}) = \sqrt{\rho_0} d_b(\mathbf{q})^{-\frac{\alpha}{2}} \tilde{\mathbf{G}}_b. \quad (76)$$

Define the following fixed gains that incorporate the beam-forming vectors $\{\mathbf{p}_k\}$:

$$\tilde{A}_{k,\ell} \triangleq \rho_0^2 \left| \tilde{\mathbf{g}}_k^H \Theta \tilde{\mathbf{G}}_b \mathbf{p}_\ell \right|^2, \quad \forall k, \ell \in \mathcal{K}, \quad (77)$$

$$\tilde{D}_{j,\ell} \triangleq \rho_0 \tilde{\mathbf{h}}_j^H \Theta \tilde{\mathbf{G}}_b \mathbf{p}_\ell, \quad \forall j \in \mathcal{J}, \forall \ell \in \mathcal{K}. \quad (78)$$

Since both the desired signal and interference powers scale with the product $(d_k(\mathbf{q})d_b(\mathbf{q}))^{-\alpha}$, it is convenient to decouple the distance-dependent terms. To this end, we introduce slack variables $\{y_{kb}\}$ and $\{y_{jb}\}$ such that

$$d_k(\mathbf{q}) d_b(\mathbf{q}) \leq y_{kb}^{\frac{1}{\alpha}}, \quad \forall k \in \mathcal{K}, \quad (79a)$$

$$d_j(\mathbf{q}) d_b(\mathbf{q}) \leq y_{jb}^{\frac{1}{\alpha}}, \quad \forall j \in \mathcal{J}. \quad (79b)$$

Although the function $y^{1/\alpha}$ is concave for $\alpha \geq 2$, the constraints in (79) remain nonconvex due to the bilinear terms $d_k(\mathbf{q})d_b(\mathbf{q})$ and $d_j(\mathbf{q})d_b(\mathbf{q})$. To construct a convex surrogate, we employ the arithmetic–geometric mean (AGM) inequality. Specifically, at iteration t , for any nonnegative variables a and b , the product ab is upper bounded as

$$ab \leq \tilde{\Theta}^{(t)}(a, b) \triangleq \frac{1}{2} \left(\frac{b^{(t-1)}}{a^{(t-1)}} a^2 + \frac{a^{(t-1)}}{b^{(t-1)}} b^2 \right), \quad (80)$$

where $(a^{(t-1)}, b^{(t-1)})$ denotes the point from the previous iteration. The surrogate $\tilde{\Theta}^{(t)}(a, b)$ is convex and tight at $(a^{(t-1)}, b^{(t-1)})$. Consequently, the slack-variable constraints admit the following convex SCA approximation

$$\tilde{\Theta}^{(t)}(d_k(\mathbf{q}), d_b(\mathbf{q})) \leq y_{kb}^{\frac{1}{\alpha}}, \quad \forall k, \quad (81)$$

$$\tilde{\Theta}^{(t)}(d_j(\mathbf{q}), d_b(\mathbf{q})) \leq y_{jb}^{\frac{1}{\alpha}}, \quad \forall j. \quad (82)$$

By multiplying both the numerator and denominator of the SINR expression by $(d_k(\mathbf{q})d_b(\mathbf{q}))^\alpha$ and using the slack variable definition in (79), the legitimate-user SINR can be conservatively represented as

$$\gamma_k(\mathbf{q}) = \frac{\tilde{A}_{k,k}}{\sum_{\ell \neq k} \tilde{A}_{k,\ell} + \sigma^2 y_{kb}}, \quad \forall k \in \mathcal{K}. \quad (83)$$

2) *SCA-Based Convex Surrogates:* Introduce auxiliary SINR variables $\{\tilde{\rho}_k\}$ and the rate variable ζ . Using (83), the rate constraints can be equivalently written as

$$\zeta \leq \log_2(1 + \tilde{\rho}_k), \quad \forall k \in \mathcal{K}, \quad (84a)$$

$$\tilde{\rho}_k \left(\sum_{\ell \neq k} \tilde{A}_{k,\ell} + \sigma^2 y_{kb} \right) \leq \tilde{A}_{k,k}, \quad \forall k \in \mathcal{K}. \quad (84b)$$

The bilinear term $\tilde{\rho}_k y_{kb}$ in (84b) is nonconvex. At iteration t , it is upper bounded by the convex AGM inequality introduced in the previous subsection as

$$\tilde{\rho}_k y_{kb} \leq \tilde{\Theta}^{(t)}(\tilde{\rho}_k, y_{kb}) \quad (85)$$

which is convex in $(\tilde{\rho}_k, y_{kb})$ and tight at $(\tilde{\rho}_k^{(t-1)}, y_{kb}^{(t-1)})$. Hence, a convex surrogate of (84b) is

$$\tilde{\rho}_k \sum_{\ell \neq k} \tilde{A}_{k,\ell} + \sigma^2 \tilde{\Theta}^{(t)}(\tilde{\rho}_k, y_{kb}) \leq \tilde{A}_{k,k}, \quad \forall k \in \mathcal{K}. \quad (86)$$

3) *Energy harvesting constraint:* The harvested RF power at UEHR j is

$$P_j^{\text{EH}}(\mathbf{q}) = \sum_{\ell=1}^K |c_{j,\ell} + x_{jb} \tilde{D}_{j,\ell}|^2, \quad \forall j \in \mathcal{J}, \quad (87)$$

where $x_{jb} \triangleq (d_j(\mathbf{q})d_b(\mathbf{q}))^{-\alpha/2}$ is the cascaded path-loss factor. The nonconvexity of (87) stems from the distance-dependent term x_{jb} . To obtain a numerically stable SCA formulation, we eliminate x_{jb} by expressing the bound in terms of x_{jb}^2 and using the relation $x_{jb}^2 \geq 1/y_{jb}$, as established in Proposition 2.

Proposition 2. Consider (87) and let y_{jb} be defined as in (79b). Define the constants $U_j \triangleq \sum_{\ell=1}^K |c_{j,\ell}|^2$, $S_j \triangleq \sum_{\ell=1}^K |\tilde{D}_{j,\ell}|^2$, and $T_j \triangleq \sum_{\ell=1}^K \Re \left\{ c_{j,\ell}^* \tilde{D}_{j,\ell} \right\}$. Then, for any

Algorithm 4: SCA-Based UAV Location Optimization

Input: Initial $\mathbf{q}^{(0)} \in \mathcal{L}$, tolerance $\varepsilon > 0$.
Output: Optimized UAV location \mathbf{q}^* .

- 1 Set $t \leftarrow 1$ and initialize $(\tilde{\rho}^{(0)}, \mathbf{y}_b^{(0)}, \mathbf{y}_u^{(0)})$ from $\mathbf{q}^{(0)}$;
- 2 **repeat**
- 3 Construct $\tilde{\Theta}^{(t)}(\cdot)$ and $\tilde{\psi}_j^{(t)}(\cdot)$ using (85) and (89);
- 4 Solve (91) to obtain $(\mathbf{q}^{(t)}, \zeta^{(t)})$;
- 5 Update the linearization points and set $t \leftarrow t + 1$;
- 6 **until** $|\zeta^{(t)} - \zeta^{(t-1)}| \leq \varepsilon$;
- 7 **return** $\mathbf{q}^{(t-1)}$;

$\varepsilon_j > 1/S_j$ (when $S_j > 0$), the harvested power admits the global lower bound

$$P_j^{\text{EH}}(\mathbf{q}) \geq A_j(\varepsilon_j) + B_j(\varepsilon_j) \frac{1}{y_{jb}}, \quad \forall j \in \mathcal{J}, \quad (88)$$

where $A_j(\varepsilon_j) \triangleq U_j - \varepsilon_j T_j^2$, and $B_j(\varepsilon_j) \triangleq S_j - \frac{1}{\varepsilon_j} > 0$.

Proof. See Appendix B. \blacksquare

Using (88), the EH requirement can be enforced in SCA by linearizing $1/y_{jb}$ around the previous iterate. Since $h(y) = 1/y$ is convex for $y > 0$, its first-order Taylor approximation at $y_{jb}^{(t-1)}$ is a global affine underestimator

$$\frac{1}{y_{jb}} \geq \frac{1}{y_{jb}^{(t-1)}} - \frac{1}{(y_{jb}^{(t-1)})^2} (y_{jb} - y_{jb}^{(t-1)}) \triangleq \tilde{\psi}_j^{(t)}(y_{jb}). \quad (89)$$

Therefore, a sufficient convex inner approximation of the EH constraint (50b) is

$$\sum_{j \in \mathcal{J}} \left(A_j(\varepsilon_j) + B_j(\varepsilon_j) \tilde{\psi}_j^{(t)}(y_{jb}) \right) \geq \Omega^{-1}(E_h). \quad (90)$$

Remark 2. A simple and stable choice of ε_j is $\varepsilon_j = \frac{2}{S_j}$ (for $S_j > 0$), which yields $B_j(\varepsilon_j) = S_j/2$ and $A_j(\varepsilon_j) = U_j - 2T_j^2/S_j$.

4) *Convex UAV Subproblem:* At SCA iteration t , the UAV location is updated by solving

$$\max_{\tilde{\mathbf{q}}} \zeta \quad (91a)$$

$$\text{s.t. } (84a), (86), (81), (82), (90), (36d). \quad (91b)$$

Here the optimization variable set is $\tilde{\Xi} \triangleq \{\mathbf{q}, \zeta, \tilde{\rho}, \mathbf{y}_b, \mathbf{y}_u\}$, where $\tilde{\rho} = \{\tilde{\rho}_k\}_{k \in \mathcal{K}}$, $\mathbf{y}_b = \{y_{kb}\}_{k=1}^K$, and $\mathbf{y}_u = \{y_{jb}\}_{j=1}^J$. The proposed method for UAV location optimization is summarized in Algorithm 4. Problem (91) is convex and can be efficiently solved using standard convex optimization solvers (e.g., CVX). The linearization points $\{\tilde{\rho}_k^{(t)}, y_{kb}^{(t)}, y_{jb}^{(t)}\}$ are updated iteratively after each solve until convergence.

By alternately optimizing the power allocation, RIS reflection phases, and UAV location, the benchmark problem in (50) can be efficiently solved via a BCD framework, where each block is handled using the SCA-based procedures developed in Sections IV-A, IV-B, and IV-C. The complete procedure is summarized in Algorithm 5.

Algorithm 5: BCD–SCA Benchmark for WCSEE Maximization

Input: Initial feasible $\tilde{\mathbf{p}}^{(0)} \succeq \mathbf{0}$, $\mathbf{s}^{(0)}, \mathbf{q}^{(0)} \in \mathcal{L}$; tolerances $\epsilon_{\text{out}} > 0$, $\epsilon_D > 0$, $\epsilon_S > 0$; penalty weight $C > 0$; maximum outer iterations I_{\max} .
Output: $\tilde{\mathbf{p}}^*, \mathbf{s}^*$ (hence Θ^*), and \mathbf{q}^* .

- 1 Set $i \leftarrow 0$ and initialize $\eta^{(0)} \leftarrow 0$.
- 2 **repeat**
- 3 Update the effective channel \mathbf{H}_c using $\mathbf{s}^{(i)}$ and $\mathbf{q}^{(i)}$, and compute ZF directions $\{\hat{\mathbf{p}}_k^{(i)}\}$ via (14)–(16).
- 4 Update $\tilde{\mathbf{p}}^{(i+1)}$ by Algorithm 2 with given $\mathbf{s}^{(i)}$ and $\mathbf{q}^{(i)}$.
- 5 Update $\mathbf{s}^{(i+1)}(\Theta^{(i+1)})$ by Algorithm 3 with given $\{\mathbf{p}_k^{(i+1)}\}$ and $\mathbf{q}^{(i)}$.
- 6 Update $\mathbf{q}^{(i+1)}$ by Algorithm 4 with given $\{\mathbf{p}_k^{(i+1)}\}$ and $\Theta^{(i+1)}$.
- 7 Evaluate the minimum secrecy rate $R^{\text{sec},(i+1)}$ using (35) and (28);
- 8 Update $\eta^{(i+1)} \leftarrow \frac{R^{\text{sec},(i+1)}}{\varrho \sum_{k=1}^K \tilde{p}_k^{(i+1)} + P_0}$;
- 9 $i \leftarrow i + 1$.
- 10 **until** $|\eta^{(i)} - \eta^{(i-1)}| \leq \epsilon_{\text{out}}$ **or** $i = I_{\max}$
- 11 **return** $\tilde{\mathbf{p}}^{(i)}, \mathbf{s}^{(i)}$, and $\mathbf{q}^{(i)}$.

V. NUMERICAL RESULTS

This section evaluates the performance of the proposed SAC-based algorithm and compares it with SCA- and DDPG-based benchmarks under various system settings. The results confirm that the SAC approach consistently achieves superior performance across different scenarios.

A. Simulation and Benchmark Settings

Unless otherwise specified, simulations are conducted in a $1500 \times 3000 \text{ m}^2$ area with the BS located at $(0, 0)$ and a UAV-mounted RIS initially positioned at $(1000, 0, 100)$ m. The UAV moves horizontally within a $50 \times 50 \text{ m}^2$ region at a fixed altitude of $H = 100$ m. The BS employs $N_t = 6$ antennas to serve $K = 4$ legitimate users in the presence of $J = 3$ UEHRs, randomly distributed within circles of radius 500 m. The RIS consists of $M = 10$ elements with discrete phase resolution $L = 8$. Unless stated otherwise, $P_{\max} = 10 \text{ dBm}$, $\sigma^2 = 10^{-3}$, $P_0 = 1 \text{ W}$, and $\alpha = 2.5$. Both perfect and ICSI are considered; for ICSI, the uncertainty radius is $\nu \in [0.01, 0.1]$, and the minimum harvested energy requirement is $E_h \in [0.005, 0.02]$. For SCA, results are averaged over 100 channel realizations with tolerance $\epsilon = 0.01$. For DRL-based methods, each run consists of $T = 2 \times 10^4$ interaction steps, and results are averaged over multiple random seeds. The main hyperparameters are summarized in Table I.

B. Performance in the Ideal Case

We first evaluate the performance of the SCA, DDPG, and the proposed SAC algorithms under an ideal setting with

TABLE I
HYPERPARAMETERS FOR SAC/DDPG-BASED ALGORITHMS

Parameter	Description	Value
Loss	Critic loss function	MSE
γ	Discount factor	0.99
τ	Target-network soft update factor	5×10^{-3}
B	Mini-batch size	256
D	Replay buffer size	10^5
T	Training steps per episode	2×10^4
Activation	Hidden-layer activation	ReLU
Hidden layers	Number of hidden layers	2
Hidden units	Units per hidden layer	256
λ_π	Actor learning rate	10^{-4}
λ_Q	Critic learning rate	10^{-3}
λ_β	Temperature learning rate	10^{-3} (SAC)

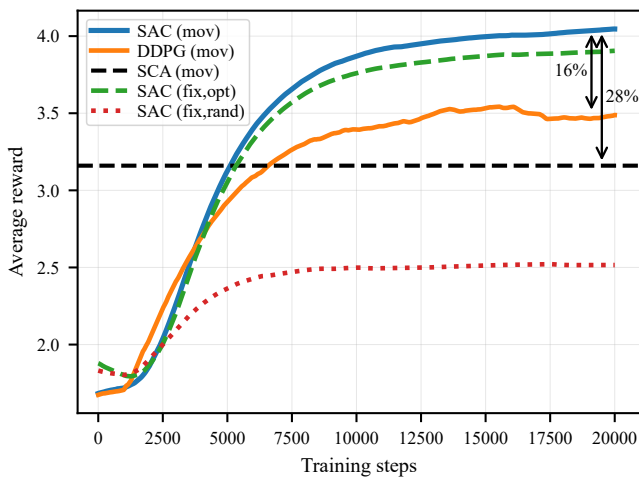


Fig. 3. Convergence behavior under the ideal setting at $P_{\max} = 10$ dBm.

PCSI and continuous RIS phase shifts, which serves as a performance benchmark under ideal conditions.

As shown in Fig. 3, the proposed SAC-based method with a movable RIS achieves the highest total reward and fastest convergence. At convergence, SAC outperforms the SCA benchmark by approximately 28% and DDPG by about 16%. This gain stems from SAC's ability to jointly optimize RIS phases, UAV location, and transmit power within a single learning framework, whereas SCA relies on sequential updates and approximations that may converge to suboptimal solutions. The figure also includes two additional benchmarks with a fixed RIS: (i) *SAC (fix,opt)* with optimized RIS phases and (ii) *SAC (fix,rand)* with random phases. The results highlight the importance of RIS phase optimization, as random phases significantly degrade performance due to the loss of control over the cascaded BS–RIS–IHR/UEHR links.

Fig. 4 depicts SEE versus the transmit power P_{\max} for the SCA, DDPG, and the proposed SAC-based schemes. As expected, increasing the transmit power improves the SEE for all methods due to the enhanced achievable secrecy rates. Nevertheless, the proposed SAC-based approach consistently outperforms both SCA and DDPG over the entire transmit power range. At high transmit power levels, the performance of SCA becomes comparable to that of DDPG; however, both remain inferior to the proposed SAC-based algorithm.

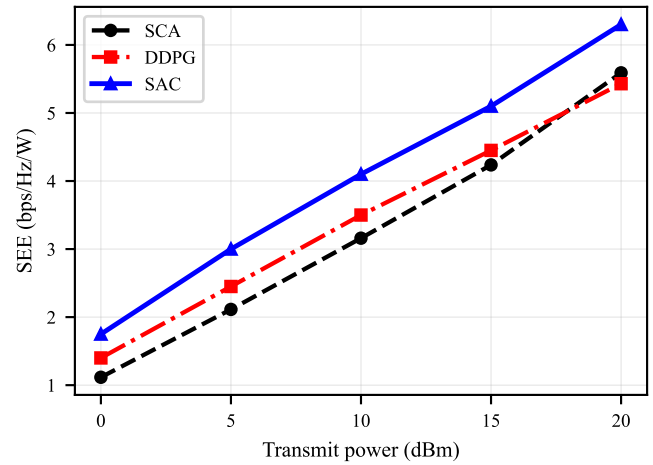


Fig. 4. SEE versus transmit power for SCA, DDPG, and the proposed SAC-based scheme.

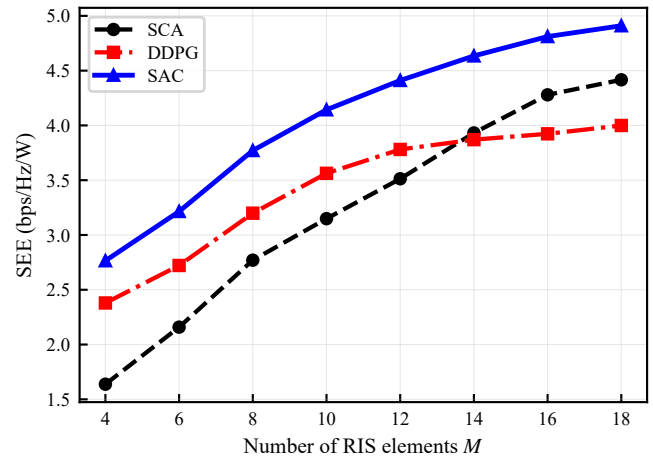


Fig. 5. SEE versus the number of RIS elements M at $P_{\max} = 10$ dBm for different schemes.

Fig. 5 illustrates the impact of the number of RIS elements M on the SEE under the ideal PCSI setting. It is observed that SEE improves monotonically with M for all schemes, since a larger RIS provides higher passive beamforming gain and stronger cascaded links. The proposed SAC-based approach consistently achieves the highest SEE across the entire range of M , demonstrating its effectiveness in jointly optimizing RIS phase shifts, UAV location, and transmit power. In contrast, the SCA-based benchmark exhibits faster improvement at larger M due to the increasing accuracy of optimization under PCSI, while the DDPG-based method shows earlier saturation, indicating limited adaptability to the expanded action space. Overall, the results confirm the superior scalability and robustness of SAC in exploiting larger RIS apertures.

C. Performance in the Non-Ideal Case

We next evaluate a non-ideal setting with ICSI and discrete RIS phases ($L = 8$), where $E_h = 0.02$ and $P_{\max} = 10$ dBm.

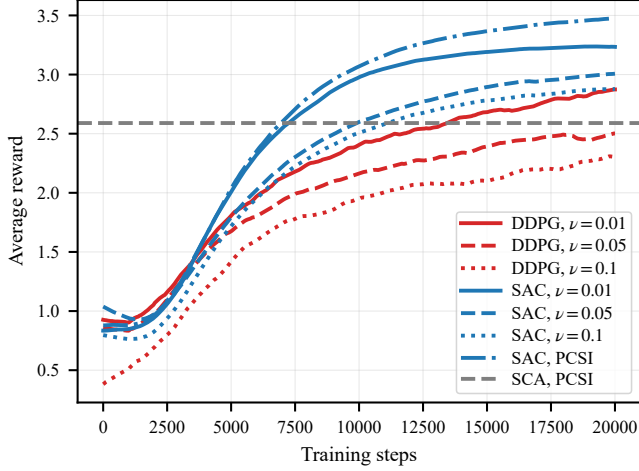


Fig. 6. Convergence comparison under ICSI with discrete RIS phases ($L = 8$) and $E_h = 0.02$ at $P_{\max} = 10$ dBm.

Fig. 6 compares SAC and DDPG for different CSI uncertainty radii $\nu \in \{0.01, 0.05, 0.1\}$, with PCSI curves and the SCA (PCSI) baseline shown for reference. It can be observed that increasing ν reduces the achievable reward due to conservative robust design. Nevertheless, SAC consistently outperforms DDPG across all uncertainty levels and converges faster. Notably, SAC with $\nu = 0.1$ still exceeds the performance of DDPG with $\nu = 0.01$, demonstrating the robustness of the proposed method under severe CSI uncertainty. This performance gain is mainly attributed to the entropy-regularized policy update and the twin-critic architecture in SAC, which mitigate value overestimation and enhance exploration stability in the presence of CSI uncertainty.

Finally, Fig. 7 compares the learning performance of SAC and DDPG under different mini-batch sizes B with $\nu = 0.01$, $P_{\max} = 10$ dBm, and $E_h = 0.01$. It is observed that the proposed SAC algorithm consistently achieves higher average rewards and faster convergence than DDPG for all considered batch sizes. Moreover, increasing B leads to smoother learning curves and improved convergence stability for both methods, since larger batches yield more accurate gradient estimates and reduce the variance of stochastic updates. Nevertheless, even with small mini-batch sizes, SAC exhibits superior robustness and stability compared with DDPG, highlighting its stronger sample efficiency and suitability for robust UAV-RIS optimization.

VI. CONCLUSIONS AND FUTURE WORK

This paper investigated secure downlink transmission in a UAV-mounted RIS-assisted multiuser MISO network with UEHRs. A WCSEE maximization problem was formulated under ICSI, discrete RIS phase constraints, and UAV mobility, jointly involving transmit power allocation, RIS phase control, and UAV positioning. A SAC-based DRL framework was proposed to solve the resulting highly nonconvex problem without convex approximations. In addition, an SCA-based BCD solution was derived for the ideal PCSI case with

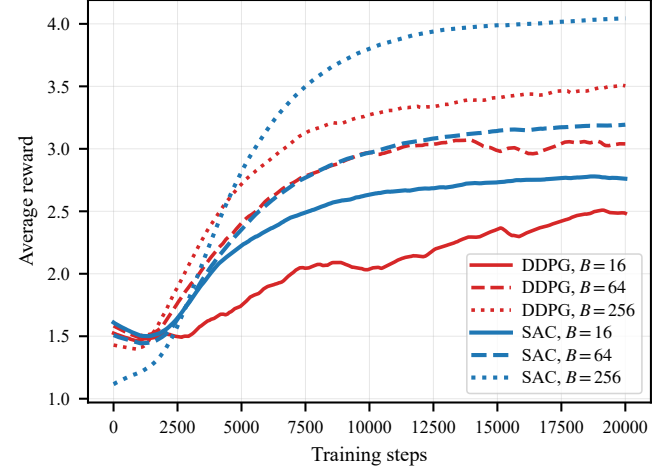


Fig. 7. Convergence comparison of SAC and DDPG under different mini-batch sizes B with $\nu = 0.01$, $P_{\max} = 10$ dBm, and $E_h = 0.01$.

continuous RIS phases as a benchmark. Simulation results showed that the proposed SAC approach achieves approximately 28% and 16% SEE gains over SCA and DDPG, respectively, under ideal conditions. In non-ideal scenarios, SAC consistently provides faster convergence and higher SEE, and remains robust to severe CSI uncertainty, where SAC with $\nu = 0.1$ outperforms DDPG with $\nu = 0.01$. Moreover, SAC maintains superior performance across a wide transmit power range. Future work will extend this framework to multi-UAV deployments and dynamic environments with time-varying CSI and user mobility.

APPENDIX A PROOF OF PROPOSITION 1

We outline the derivations of (68a)–(68e).

A) Derivation of (68a)

The legitimate SINR constraint in (66a) can be expressed (after introducing ρ_k) as

$$\rho_k \leq \frac{|\mathbf{t}_{kk}^H \mathbf{s}|^2}{\sum_{\ell \neq k} |\mathbf{t}_{k\ell}^H \mathbf{s}|^2 + \sigma^2}, \quad \forall k \in \mathcal{K}. \quad (\text{A.1})$$

Rearranging (A.1) yields the DC form

$$\mathcal{M}_k(\mathbf{s}) - \mathcal{N}_k(\mathbf{s}, \rho_k) \leq 0, \quad (\text{A.2})$$

where $\mathcal{M}_k(\mathbf{s}) \triangleq \sum_{\ell \neq k} |\mathbf{t}_{k\ell}^H \mathbf{s}|^2 + \sigma^2$ and $\mathcal{N}_k(\mathbf{s}, \rho_k) \triangleq \frac{|\mathbf{t}_{kk}^H \mathbf{s}|^2}{\rho_k}$. The nonconvexity is due to $\mathcal{N}_k(\mathbf{s}, \rho_k)$. Thus, at iteration t , we replace $\mathcal{N}_k(\mathbf{s}, \rho_k)$ by its first-order Taylor approximation $\Psi^{(t)}(\mathbf{s}, \rho_k; \mathbf{t}_{kk})$, which directly gives (68a).

B) Derivation of (68b)–(68c)

For UEHR j decoding user k , introduce auxiliary variables $\rho_{E,j,k}$ and $\xi_{j,k}$ such that

$$\begin{cases} |c_{j,k} + \mathbf{t}_{j,k}^H \mathbf{s}|^2 \leq \xi_{j,k} \rho_{E,j,k}, \\ \xi_{j,k} \leq \sum_{\ell \neq k} |c_{j,\ell} + \mathbf{t}_{j,\ell}^H \mathbf{s}|^2 + \sigma^2. \end{cases} \quad (\text{A.3})$$

The product $\xi_{j,k}\rho_{E,j,k}$ in (A.3) is bilinear and nonconvex; we apply the standard affine lower bound $\Theta^{(t)}(\xi_{j,k}, \rho_{E,j,k})$, which yields (68b). Moreover, each quadratic term $|c_{j,\ell} + \mathbf{t}_{j,\ell}^H \mathbf{s}|^2$ in the second inequality of (A.3) is convex; hence, we upper bound it by its first-order Taylor expansion $\vartheta^{(t)}(c_{j,\ell}, \mathbf{t}_{j,\ell}; \mathbf{s})$, leading to (68c).

C) Derivation of (68d)–(68e)

Constraint (68d) follows by rewriting $f_{E,k} \geq \log_2(1 + \rho_{E,j,k})$ into $2^{f_{E,k}} \geq 1 + \rho_{E,j,k}$ and then applying the first-order Taylor approximation $\Gamma^{(t)}(f_{E,k})$ of $2^{f_{E,k}}$. Finally, (68e) is the epigraph form of the secrecy constraint. This completes the proof.

APPENDIX B PROOF OF PROPOSITION 2

For fixed $\{c_{j,\ell}, \tilde{D}_{j,\ell}\}$ and real $x_{jb} \geq 0$, expanding (87) yields the convex quadratic

$$P_j^{\text{EH}}(x_{jb}) = U_j + S_j x_{jb}^2 + 2T_j x_{jb}, \quad (\text{B.1})$$

where U_j , S_j , and T_j are defined in Proposition 2. Next, we lower bound the linear term $2T_j x_{jb}$.

Lemma 1. For any $x_{jb} \in \mathbb{R}$ and any $\varepsilon_j > 0$,

$$2T_j x_{jb} \geq -\varepsilon_j T_j^2 - \frac{1}{\varepsilon_j} x_{jb}^2. \quad (\text{B.2})$$

Proof. Let $a = \sqrt{\varepsilon_j} T_j$ and $b = x_{jb}/\sqrt{\varepsilon_j}$. Since $(a+b)^2 \geq 0$, we have $2ab \geq -a^2 - b^2$, i.e., $2T_j x_{jb} \geq -\varepsilon_j T_j^2 - x_{jb}^2/\varepsilon_j$, which proves (B.2). \blacksquare

Applying Lemma 1 to (B.1) yields, for any $\varepsilon_j > 0$,

$$P_j^{\text{EH}} \geq (U_j - \varepsilon_j T_j^2) + \left(S_j - \frac{1}{\varepsilon_j}\right) x_{jb}^2 = A_j(\varepsilon_j) + B_j(\varepsilon_j) x_{jb}^2. \quad (\text{B.3})$$

Choosing $\varepsilon_j > 1/S_j$ (for $S_j > 0$) ensures $B_j(\varepsilon_j) > 0$. Finally, from (79b) and $x_{jb} = (d_j^2(\mathbf{q})d_b^2(\mathbf{q}))^{-\alpha/4}$, we obtain

$$x_{jb}^2 = (d_j^2(\mathbf{q})d_b^2(\mathbf{q}))^{-\alpha/2} \geq \frac{1}{y_{jb}}. \quad (\text{B.4})$$

Substituting (B.4) into (B.3) yields $P_j^{\text{EH}} \geq A_j(\varepsilon_j) + B_j(\varepsilon_j) 1/y_{jb}$, which coincides with (88) and completes the proof.

REFERENCES

- [1] R. Kaur, et al., “A Survey on Reconfigurable Intelligent Surface for Physical Layer Security of Next-Generation Wireless Communications,” *IEEE Open J. Veh. Technol.*, vol. 5, pp. 172-199, 2024.
- [2] U. A. Mughal, et al., “Deep Learning for Secure UAV-Assisted RIS Communication Networks,” *IEEE Internet Things Mag.*, vol. 7, no. 2, pp. 38-44, March 2024.
- [3] S. Li, et al., “Robust Secure UAV Communications With the Aid of Reconfigurable Intelligent Surfaces,” *IEEE Trans. Wirel. Commun.*, vol. 20, no. 10, pp. 6402-6417, Oct. 2021.
- [4] Y. Shang, et al., “RIS-Assisted Secure UAV Communication Scheme Against Active Jamming and Passive Eavesdropping,” *IEEE Trans. Intell. Transp. Syst.*, vol. 25, no. 11, pp. 16953-16963, Nov. 2024.
- [5] B. Zhang, et al., “Performance Analysis of RIS-Assisted Wireless Communications With Energy Harvesting,” *IEEE Trans. Veh. Technol.*, vol. 72, no. 1, pp. 1325-1330, Jan. 2023.
- [6] M. Mohammadi, H. Q. Ngo and M. Matthaiou, “Phase-Shift and Transmit Power Optimization for RIS-Aided Massive MIMO SWIPT IoT Networks,” *IEEE Trans. Commun.*, vol. 73, no. 1, pp. 631-647, Jan. 2025.
- [7] J. Ouyang, et al., “Secrecy Energy Efficiency in Full-Duplex AF Relay Systems With Untrusted Energy Harvesters,” *IEEE Commun. Lett.*, vol. 25, no. 11, pp. 3493-3497, Nov. 2021.
- [8] H. R. Hashempour et al., “Secure SWIPT in the Multiuser STAR-RIS Aided MISO Rate Splitting Downlink,” *IEEE Trans. Veh. Technol.*, vol. 73, no. 9, pp. 13466-13481, Sept. 2024.
- [9] J. Li, D. Wang, H. Zhao, Y. Jin, and Y. He, “Enhancing secrecy energy efficiency in UAV-RIS assisted mobile IoV networks through deep reinforcement learning,” *IEEE Trans. Wirel. Commun.*, doi: 10.1109/TWC.2025.3594691.
- [10] M. Amiri, A. Mohammadi, F. Zeinali, M. R. Mili, M. B. Mashhadi, and P. Xiao, “Movable antenna SWIPT systems with STAR-RIS: A meta deep reinforcement learning approach,” *IEEE Trans. Veh. Technol.*, doi: 10.1109/TVT.2025.3622305.
- [11] C. Luo, W. Jiang, D. Niyato, Z. Ding, J. Li, and Z. Xiong, “Optimization and DRL-based joint beamforming design for active-RIS enabled cognitive multicast systems,” *IEEE Trans. Wirel. Commun.*, vol. 23, no. 11, pp. 16234-16247, Nov. 2024.
- [12] Z. Shi, H. Lu, X. Xie, H. Yang, C. Huang, J. Cai, and Z. Ding, “Active RIS-aided EH-NOMA networks: A deep reinforcement learning approach,” *IEEE Trans. Commun.*, vol. 71, no. 10, pp. 5846-5861, Oct. 2023.
- [13] Y. Zhang, et al., “Deep Reinforcement Learning for Secrecy Energy Efficiency Maximization in RIS-Assisted Networks,” *IEEE Trans. Veh. Technol.*, vol. 72, no. 9, pp. 12413-12418, Sept. 2023.
- [14] M. M. Razaq and L. Peng, “DRL-based physical-layer security optimization in near-field MIMO systems,” *IEEE Internet Things J.*, vol. 12, no. 12, pp. 18606-18615, 15 June 15, 2025.
- [15] Z. Ma, R. Zhang, B. Ai, Z. Lian, L. Zeng, D. Niyato, and Y. Peng, “Deep reinforcement learning for energy efficiency maximization in RSMA-IRS-assisted ISAC systems,” *IEEE Trans. Wireless Commun.*, vol. 74, no. 11, pp. 18273-18278, Nov. 2025.
- [16] H. Fu, S. Feng, W. Tang, and D. W. K. Ng, “Robust secure beamforming design for two-user downlink MISO rate-splitting systems,” *IEEE Trans. Wirel. Commun.*, vol. 19, no. 12, pp. 8351-8365, Dec. 2020.
- [17] E. Boshkovska, D. W. K. Ng, N. Zlatanov, A. Koelpin and R. Schober, “Robust resource allocation for MIMO wireless powered communication networks based on a non-linear EH model,” *IEEE Trans. Commun.*, vol. 65, no. 5, pp. 1984-1999, May 2017.
- [18] E. A. Gharavol, Y. Liang and K. Moushaan, “Robust downlink beamforming in multiuser MISO cognitive radio networks with imperfect channel-state information,” *IEEE Trans. Veh. Technol.*, vol. 59, no. 6, pp. 2852-2860, July 2010.
- [19] E. Boshkovska, et al., “Practical Non-Linear Energy Harvesting Model and Resource Allocation for SWIPT Systems,” *IEEE Commun. Lett.*, vol. 19, no. 12, pp. 2082-2085, Dec. 2015.
- [20] L. D. Nguyen, et al., “Energy Efficiency in Cell-Free Massive MIMO with Zero-Forcing Precoding Design,” *IEEE Commun. Lett.*, vol. 21, no. 8, pp. 1871-1874, Aug. 2017.
- [21] T. Haarnoja, A. Zhou, P. Abbeel, and S. Levine, “Soft actor-critic: Off-policy maximum entropy deep reinforcement learning with a stochastic actor,” *Proc. IEEE Int. Conf. Mach. Learn.*, 2018, pp. 1861-1870.
- [22] T. Haarnoja et al., “Soft actor-critic algorithms and applications,” 2018, *arXiv:1812.05905*. [Online]. Available: <http://arxiv.org/abs/1812.05905>.
- [23] W. Dinkelbach, “On nonlinear fractional programming,” *Manage. Sci.*, vol. 13, no. 7, pp. 492-498, Mar. 1967.
- [24] V. Kumar, R. Zhang, M. D. Renzo, and L.-N. Tran, “A Novel SCA-Based Method for Beamforming Optimization in IRS/RIS-Assisted MU-MISO Downlink,” *IEEE Wirel. Commun. Lett.*, vol. 12, no. 2, pp. 297-301, Feb. 2023.
- [25] H. Long et al., “Joint Trajectory and Passive Beamforming Design for Secure UAV Networks with RIS,” *2020 IEEE Globecom Workshops (GC Wkshps, Taipei, Taiwan*, 2020, pp. 1-6.